

ExPath: Targeted Pathway Inference for Biological Knowledge Bases via Graph Learning and Explanation

Rikuto Kotoge*
SANKEN, Osaka University
Osaka, Japan
rikuto88@sanken.osaka-u.ac.jp

Ziwei Yang*
Kyoto University
Kyoto, Japan
yang.ziwei.37j@st.kyoto-u.ac.jp

Zheng Chen†
SANKEN, Osaka University
Osaka, Japan
chenz@sanken.osaka-u.ac.jp

Yushun Dong†
Florida State University
Tallahassee, FL, USA
yd24f@fsu.edu

Yasuko Matsubara
SANKEN, Osaka University
Osaka, Japan
yasuko@sanken.osaka-u.ac.jp

Jimeng Sun
University of Illinois
Urbana-Champaign
Urbana, IL, USA
jimeng@illinois.edu

Yasushi Sakurai
SANKEN, Osaka University
Osaka, Japan
yasushi@sanken.osaka-u.ac.jp

ABSTRACT

Biological knowledge bases provide systemically functional pathways of cells or organisms in terms of molecular interaction. However, recognizing more targeted pathways, particularly when incorporating wet-lab experimental data, remains challenging and typically requires downstream biological analyses and expertise. In this paper, we frame this challenge as a solvable graph learning and explaining task and propose a novel pathway inference framework, ExPath, that explicitly integrates experimental data, specifically amino acid sequences (AA-seqs), to classify various graphs (bio-networks) in biological databases. The links (representing pathways) that contribute more to classification can be considered as targeted pathways. Technically, ExPath comprises three components: (1) a large protein language model (pLM) that encodes and embeds AA-seqs into graph, overcoming traditional obstacles in processing AA-seq data, such as BLAST; (2) PathMamba, a hybrid architecture combining graph neural networks (GNNs) with state-space sequence modeling (Mamba) to capture both local interactions and global pathway-level dependencies; and (3) PathExplainer, a subgraph learning module that identifies functionally critical nodes and edges through trainable pathway masks. We also propose ML-oriented biological evaluations and a new metric. The experiments involving 301 bio-networks evaluations demonstrate that pathways inferred by ExPath maintain biological meaningfulness. We will publicly release curated 301 bio-network data soon. The source code is available at: <https://anonymous.4open.science/r/ExPath>

CCS CONCEPTS

• Applied computing → Bioinformatics; • Computing methodologies → Machine learning approaches.

KEYWORDS

pathway, graph, SSM, explainable, pLM, biology

1 INTRODUCTION

Decades of research have generated extensive network biology data, revealing that systems, from cells to organisms, can be considered molecular networks and have been reported in extensive literature

*indicates equal contribution.

†indicates corresponding authors.

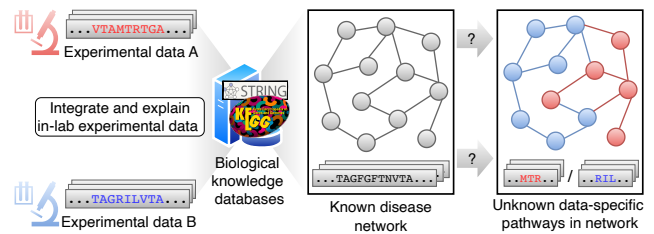


Figure 1: Biological knowledge bases lack specificity when integrating experimental data. This example illustrates two experimental datasets with different mutations that share the same disease pathway structure, yet fail to reveal the distinct interactions responsible for these differences.

[1, 6, 23]. These data resources have been compiled into functional biological knowledge bases, such as KEGG [27] and STRING [55], framing bio-network resources [32, 46] that document various interactions between molecules (e.g., genes or proteins) to describe how molecular behaviors relate to biological systems. These knowledge bases are now widely used to mine and interpret wet-lab experimental data, enabling researchers to study disease mechanisms [5], drug interactions [69], and potential therapeutic targets [37].

While biological knowledge bases are comprehensive and continuously updated, a main concern remains: they lack specificity for experimental data. The bases cannot provide the information on which interactions are more relevant to the given data, even though their main purpose is to interpret the data. As shown in Figure 1, two experimental datasets from the same disease with different mutations share the same network structure, but fail to reveal which distinct interactions account for these differences. However, inferring key molecular interactions is crucial for understanding the potential roles of genes or proteins, potentially accelerating new biomarker discovery [72]. Conceptually, in-lab experimental data, such as amino acid sequences or gene expression profiles, is typically generated under specific research objectives or experiments, often focusing on proteins or genes of interest. However, knowledge bases provide only generic networks. They collect “meaningful” molecular interactions via automated text mining and manual curation [26], but do not incorporate the specific data that “confer such meaningfulness” into the network-building

process. As a result, they cannot provide data-specific interactions, and this generalization can lead to misinterpretations of experimental results. A few complementary bio-tools, such as BLAST [2], combined with downstream analytic methods [21], can help infer bio-networks. However, these tools are not user-friendly for non-experts, as they require domain expertise for implementation and information management [40]. Moreover, the downstream analysis generally provides empirical explanations for the data, and sometimes, extensive in-lab evaluation, such as pairwise examinations among hundreds to thousands of genes [68], is needed. There is thus an urgent need for a method that integrates bio-network resources with experimental data to infer targeted interactions, thereby facilitating the efficient use of knowledge bases.

Bio-network inference, including computational and learning-based methods, has emerged as a promising solution for mining targeted interactions. Such bio-network inference has attracted great attention from both computational biology and machine learning researchers [30, 62]. Existing methods typically form bio-network topology as graph data, embed experimental data as node features, and define proper objective functions to infer meaningful subgraphs. Computational methods typically incorporate statistical node-centric metrics in graph theory, such as node degrees [31, 33], centrality [20, 60], betweenness [44], or PageRank scores [24, 41], to evaluate the importance of nodes within a graph. The edges connecting these top-ranked nodes, or those highlighted during node evaluations, can be identified as more targeted interactions. However, such objectives lack explicit inference of interactions, i.e., edges, and are often computationally intractable for large bio-networks [45]. Moreover, computational methods cannot fully exploit experimental data, as the statistical metrics do not integrate node features into scoring schemes. By contrast, machine learning methods, particularly graph neural networks (GNNs), model both network topology and node-level attributes for subgraph inference in a data-driven manner [49, 61]. These methods set up objective functions such as link prediction and graph reconstruction to explicitly infer targeted interactions. More importantly, experimental data can directly influence the objective functions through node aggregation in GNN learning, ensuring that the model outputs are more specific to the data. However, most existing works are task-specific, and their objectives aim to learn the general graph structure accurately, including irrelevant interactions [62, 71]. Some works propose to gradually infer subgraph structure, mitigating the constraints of prior general bio-network information [30, 36]. Nonetheless, they do not explicitly learn the distinct interactions unique to different experimental data. Furthermore, existing methods typically require downstream biological analysis to interpret the model outputs or interactions. We acknowledge that current explorations in bio-network inference remain nascent.

In this paper, we study a novel and critical problem of developing a bio-network inference framework that explicitly generates data-specific interactions while maintaining biological plausibility. We note that this is a non-trivial task. In essence, we mainly face three challenges. (1) *Qualitative interaction inference objective*. The first challenge involves formulating a new objective that not only learns but also qualitatively assesses interactions directly. The model outputs, therefore, enable the direct interpretation of targeted interactions, eliminating the need for downstream analysis.

(2) *Pathway modeling*. One primary focus of knowledge bases is on “pathways” [26], i.e., connected multi-interactions, representing a sequence of events where one protein interaction triggers the next, ultimately leading to a defined outcome. However, existing works often treat all interactions equally and uniformly, focusing primarily on isolated interactions. A reliable method should explicitly incorporate pathway information into the modeling process to maintain biological plausibility. (3) *ML-oriented evaluation*. Currently, there is no standardized quantitative evaluation framework tailored for machine learning models. Most evaluations depend on qualitative methods, such as enrichment analysis [21], to determine whether the resulting interactions are biologically relevant, which requires domain expertise. A quantitative evaluation method, designed to directly assess the model outputs, would bridge the gap between computational and biological disciplines.

In this paper, we present ExPath, a deep learning framework for inferring targeted pathways for bio-networks. To tackle the above challenges, (1) we formulate bio-network inference as a subgraph learning and explanation task. Subgraphs, contributing most significantly to the learning objective, can be identified as targeted interactions. (2) To ensure these subgraphs capture high-order pathways, technically, we propose two novel models: PathMamba, a hybrid learning model, combines graph neural networks (GNNs) with state-space sequence modeling (Mamba) to learn both local interactions and global pathway-level dependencies; PathExplainer, a novel variation of GNNExplainer, designed as a subgraph explanation module, identifies objective-critical pathways. We take amino acid (AA) sequences as the reference experimental data since many biological databases organize pathway information at the protein level [15]. We utilize a large protein language model (pLM) (ESM-2 [38]) to encode AA sequences into graph embeddings, driving ExPath to mine targeted pathways effectively. (3) We propose an evaluation workflow that directly incorporates model-derived weights of subgraphs to quantitatively assess their biological significance. Overall, our contributions are:

- **Formulating Bio-network Inference Problem.** We formulate and make an initial investigation on a novel research problem of inferring data-specific pathways for bio-networks.
- **Proposing New Framework.** ExPath consists of PathMamba and PathExplainer, tailored for pathway-level modeling, can interpret data directly. It achieves the best fidelity+ and fidelity-across 10 baselines, showing both sufficiency and necessity.
- **Impacting Biological Relevance.** We propose ML-oriented biological evaluations and a new metric. The experiments involving 301 bio-networks evaluations demonstrate that pathways inferred by ExPath maintain biological meaningfulness.
- **Datasets.** We collected all available human networks from the KEGG, constructed machine-learning-ready datasets, and will release them soon.

2 PRELIMINARY AND PROBLEM SETTING

2.1 Pathways in Biological Knowledge Bases

Knowledge bases organize these pathways as interconnected graphs, where nodes represent proteins and edges denote interactions (e.g., enzymatic reactions, regulatory effects). These pathways help researchers understand how different molecules work together rather

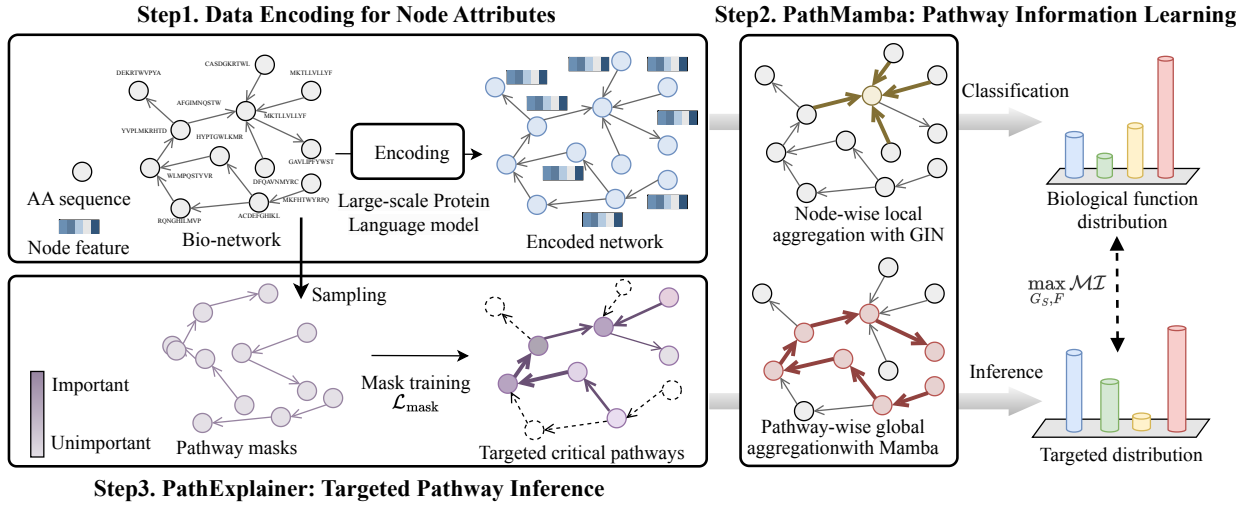


Figure 2: Overview of ExPath. ExPath comprises three components. (1) Data encoding with a large protein language model and RWPE for node attributes (AA sequences) learning; (2) PathMamba combining graph neural networks with state-space sequence modeling (Mamba) to capture both local interactions and global pathway-level dependencies for pathway information learning; and (3) PathExplainer identifies functionally critical nodes and edges through trainable pathway masks for targeted pathway inference.

than looking at just one interaction at a time. For example, while protein-protein interactions (PPI) [46] capture pair-wise molecular associations, pathways show how many proteins are linked in complex networks. This helps scientists see the “big picture,” revealing how different parts of a cell cooperate to perform important tasks [26]. Learning from amino acid (AA) sequence data is challenging due to its inherent complexity. Even slight variations can lead to significant structural changes, potentially disrupting protein functionality within pathways. Several studies focus on extracting meaningful features from AA sequences, like like AlphaFold [25]. In this paper, we investigate the mapping of AA sequence data to corresponding pathway bio-networks.

2.2 Problem Setting

Definition 1 (Amino Acid sequence data). Consider a collection of M AA sequences, denoted as $S = \{S^{(m)}\}_{m=1}^M$, where each sequence $S^{(m)}$ has a length $L^{(m)}$ (which may vary across m) and is represented as $S^{(m)} = [s_1^{(m)}, s_2^{(m)}, \dots, s_{L^{(m)}}^{(m)}]$. Here, each amino acid $s_i^{(m)}$ belongs to the standard set of 20 canonical amino acids. **Definition 2 (Knowledge bio-networks).** The bio-networks can be represented as a graph $\mathcal{G} = (\mathcal{V}, \mathcal{E})$, where \mathcal{V} denotes the vertices (e.g., AA sequences) and \mathcal{E} is the set of edges, representing molecular interactions. Let $\mathcal{G} = \{\mathcal{G}^{(m)}\}_{m=1}^M$ denote a dataset comprising M bio-networks. Each $\mathcal{G}^{(m)}$ is associated with a label $y^{(m)} \in \mathcal{Y}$, indicating its primary biological functional class (e.g., metabolism, genetic information processing, and human diseases).

Problem (Targeted Pathway Inference). We frame this research problem as a two-phase graph learning and subgraph explanation task. Given \mathcal{G} and the labels \mathcal{Y} , we focus on two main tasks:

- **Task-1 (Classification):** Train a classifier $F(\cdot)$ to predict the function label $y^{(m)}$ of an unseen bio-network $\mathcal{G}^{(m)}$, driven by the node features, i.e., AA sequence data S . To perform accurate classification, it can effectively learn various pathways in biological knowledge bases.
- **Task-2 (Explanation):** For each predicted function class $y \in \mathcal{Y}$, employ an explainer $E(\cdot)$ to extract a class-specific subgraph $\hat{\mathcal{G}} \subseteq \mathcal{G}$ that highlights the most influential pathways contributing to the classification outcome.

In plain words, a subgraph learned from various biological pathways and capable of accurately predicting its associated bio-network can be considered as representing *targeted pathways*. Let $\hat{\mathcal{G}}_y = E(\mathcal{G}, y; S)$ denote subgraphs for bio-network y , integrated to experimental data S . Here, we hold three hypotheses for our method:

- **Hypothesis-1.** The classifier $F(\cdot)$ leverages bio-network topology and AA seq features to achieve high prediction accuracy while maintaining balanced performance across all classes.
- **Hypothesis-2.** The explainer $E(\cdot)$ infers subgraphs that retain high fidelity for class discrimination and exhibit distinct structures across classes, reflecting unique biological mechanisms.
- **Hypothesis-3.** Both $F(\cdot)$ and $E(\cdot)$ must maintain biologically plausible mechanisms, ensuring that the inferred subgraphs capture high-order pathways and hold biological meaningfulness.

3 PROPOSED METHOD

3.1 Framework

ExPath comprises three components: large protein model encodings, graph-based classification, and post-hoc subgraph explanation, as shown in Figure 2. First, we encode AA sequence data using a pre-trained large protein model, ESM-2 [38] (see Section 3.2), to serve as node attributes. To address (Task-1, Hypothesis-1), PathMamba, a classifier combining graph neural networks (GNNs) with state-space sequence modeling (Mamba), is to capture both local node-pair interactions and global **pathway-level dependencies** (see Section 3.3). To address (Task-2, Hypothesis-2), PathExplainer, an explainer method trained with **pathway-wise masks** (see Section 3.4), aims to identify the most influential subgraphs. We explicitly integrate pathway-level information into both models to satisfy Hypothesis-3. The large protein model ensures biologically meaningful protein representations, PathMamba leverages various pathway information in knowledge bases for robust classification, and PathExplainer highlights minimal subgraphs that drive the final predictions, offering interpretable insights into key pathways. We evaluate ExPath from both machine learning and biological perspectives, as detailed in Section 4.

3.2 Data Encoding for Node Attributes

3.2.1 Large Protein Language Model Encoding. The ESM-2 model [38], pre-trained on over 60 million AA sequences with parameter scaling up to 15 billion, is employed to encode our data. We evaluate different parameter variants of ESM-2, and the results are presented in Table 1. Formally, each $S^{(m)}$ is tokenized and passed through stacked Transformers. The output is a token vector, denoted as: $\mathbf{h}_i = \mathbf{H}_1^{(L)}$, where $\mathbf{H}_1^{(L)} \in \mathbb{R}^d$ is the embedding of the first token from the L -th (last) Transformer layer, serving as data representation.

3.2.2 Positional Encoding. To address a fundamental limitation of GNNs [64] or hybrid models [48] to distinguish nodes with identical local structures, we apply a random-walk-based positional encoding (RWPE) base on a diffusion process [14], defined as: $\mathbf{p}_i = [RW_{ii}, RW_{ii}^2, \dots, RW_{ii}^k] \in \mathbb{R}^k$ where $RW = AD^{-1}$ is the random walk operator, constructed by the adjacency matrix A and degree matrix D . For each node i , RW_{ii}^k captures the probability of returning to node i after k steps of random walk.

The final node representation combines the sequence-level features from ESM-2 and the structural information from the graph. Specifically, the sequence embedding \mathbf{h}_i and the positional encoding \mathbf{p}_i are concatenated and passed through a linear layer to obtain the final representation: $\mathbf{x}_i = \text{Linear}([\mathbf{h}_i \parallel \mathbf{p}_i])$, where $[\mathbf{h}_i \parallel \mathbf{p}_i] \in \mathbb{R}^{d+K}$ denotes the concatenation of $\mathbf{h}_i \in \mathbb{R}^d$ and $\mathbf{p}_i \in \mathbb{R}^K$. The linear transformation ensures dimensionality reduction and effective integration of both global protein sequence features and local graph structural information. This final node feature $\mathbf{x}_i \in \mathbb{R}^d$ is optimized for downstream tasks such as graph classification.

3.3 PathMamba: Pathway Information Learning

PathMamba integrates the Graph Isomorphism Network (GIN) with a novel **pathway-wise Mamba** model. It leverages the strengths of both global selective modeling mechanisms and message-passing

GNNs. Specifically, inspired by GPS [48], our model avoids early-stage information loss that could arise from using GNNs exclusively in the initial layers. We hence employ pathway-wise global aggregation in combination with an efficient Mamba mechanism [18]. At each layer, node and edge features are updated by aggregating the outputs of a pathway-wise Mamba aggregation as:

$$X^{l+1}, = \text{PathMamba}^l(X^l, A), \quad (1)$$

$$\text{computed as } X_L^{l+1}, = \text{LocalGIN}^l(X^l, A), \quad (2)$$

$$X_G^{l+1}, = \text{GlobalMamba}^l(X^l, A), \quad (3)$$

$$X^{l+1}, = \text{MLP}^l(X_L^{l+1} + X_G^{l+1}), \quad (4)$$

where $A \in \mathbb{R}^{N \times N}$ is the adjacency matrix of a graph with N nodes and E edges; $X^l \in \mathbb{R}^{N \times d}$ represents the d -dimensional node features at layer l ; LocalGIN^l is a GIN; GlobalMamba^l is a global pathway-wise aggregation layer; and MLP^l is a two-layer multilayer perceptron (MLP) used to combine local and global features.

3.3.1 Node-wise local aggregation. Node features are updated by aggregating information from their local neighbors. The GIN operation can be expressed as:

$$X_L^{l+1} = \text{ReLU} \left(W^l \cdot ((1 + \epsilon)X^l + \sum_{j \in \mathcal{N}(i)} X_j^l) \right), \quad (5)$$

where $\mathcal{N}(i)$ represents the set of neighbors of node i , W^l is the learnable weight matrix at layer l , and ϵ is a trainable parameter controlling the importance of self-loops. This ensures a high level of expressivity for local feature aggregation.

3.3.2 Pathway-wise global aggregation. To capture long-range dependencies within pathways, we propose (1) random pathway sampling and (2) sequential pathway modeling in PathMamba.

Random Pathway Sampling. Formally, for each node v_i , we randomly sample a varied, single pathway with a maximum length of L . The sampling process is defined as:

$$\mathcal{Q} = \{\mathbf{q}^i \mid \mathbf{q}^i \sim \text{Pathway}(v_i, L), |\mathbf{q}^i| \leq L\}_{i=1}^N, \quad (6)$$

where N is the number of nodes in the graph, and \mathbf{q}^i represents the sampled pathway for node v_i . Each pathway \mathbf{q}^i is a sequence of nodes $\{v_i, v_{i_1}, v_{i_2}, \dots, v_{i_L}\}$, sampled according to a random walk process [56]. The sampling process $\text{Pathway}(v_i, L)$ involves selecting a sequence of connected nodes starting from v_i . The selection of each subsequent node is determined probabilistically, guided by the graph adjacency structure.

Sequential Pathway Modeling. The forward propagation of the Mamba layer aggregates long-range dependencies along the sampled pathways. For each sampled pathway $\mathbf{q}^i \in \mathcal{Q}(X^l)$, the Mamba layer processes the pathway sequentially as:

$$\begin{aligned} \Delta_t &= \tau_\Delta(f_\Delta(\mathbf{x}_t^l)), \quad \mathbf{B}_t = f_B(\mathbf{x}_t^l), \quad \mathbf{C}_t = f_C(\mathbf{x}_t^l), \\ \mathbf{h}_t^l &= (1 - \Delta_t \cdot \mathbf{D})\mathbf{h}_{t-1}^l + \Delta_t \cdot \mathbf{B}_t \mathbf{x}_t^l \\ X_G^{l+1} &= \mathbf{C} \cdot \mathbf{h}_t^{l+1}, \end{aligned} \quad (7)$$

where \mathbf{x}_t^l is the t -th input node feature matrix in pathway \mathbf{q}^i at layer l . f_* are learnable projections and \mathbf{h}_t^e is hidden state. τ_Δ is

the softplus function. The forgetting term $(1 - \Delta_t^e \cdot \mathbf{D})$ implements a selective mechanism analogous to synaptic decay or inhibitory processes that diminish outdated or irrelevant information. Conversely, the update term $\Delta_t^e \cdot \mathbf{B}_t^e$ mirrors gating that selectively reinforces and integrates salient new information. The projection \mathbf{C}_t^e translates the internal state into observable outputs. By processing each sampled pathway individually, the Mamba layer effectively aggregates information along each pathway. The aggregated pathway representations are then combined to form the updated node features X_G^{l+1} for the next layer.

3.3.3 Graph Classification. The updated node features are aggregated using a max pooling to generate a graph representation. This representation is passed through an MLP layer for classification:

$$y = \text{MLP}(\text{MaxPooling}(\{h_{v_i}\}_{i=1}^N)), \quad (8)$$

where N is the number of nodes, and y is the predicted class label for the pathway. The model is trained using the cross-entropy loss: $\mathcal{L}_{\text{cross-entropy}} = -\sum_{i=1}^C y_i \log \hat{y}_i$, where C is the number of classes, y_i is the ground truth label, and \hat{y}_i is the prediction.

3.4 PathExplainer: Targeted Pathway Inference

PathExplainer directly infer subgraphs to generate targeted pathways by leveraging the interpretability of PathMamba. Vallina GN-Explainers [39, 65], which focus primarily on the node or edge level, often struggle to capture the global structures at the pathway level. In contrast, PathExplainer introduces a key technical novelty by **training pathway masks**, where entire pathways (i.e., sequences of connected nodes and edges) are selectively masked during training to evaluate their contributions to PathMamba.

PathExplainer formalizes the identification of important subgraphs as an optimization problem. For a given graph $G = (V, E)$, the explanation is defined as (G_S, F_S) , where $G_S \subseteq G$ is the subgraph and F_S represents the selected features. The explanation is derived by optimizing the mutual information $\mathcal{M}I(\cdot)$ between the subgraph and the model’s prediction:

$$\max_{G_S, F} \mathcal{M}I(Y, (G_S, F)) = H(Y) - H(Y | G = G_S, X = F_S), \quad (9)$$

where $H(Y)$ is the entropy of the predictions and $H(Y | G = G_S, X = F_S)$ is the conditional entropy given the explanation.

The optimization is approached by learning a pathway mask M for the sampled pathway’s edges and nodes. To enhance the interpretability and biological relevance of the pathway mask, random pathways Q are sampled as described in Section 3.3.2. For each node v_i , a single random pathway q_i of length up to L is sampled. These pathways are then used to restrict the mask learning process to edges within the sampled pathways, ensuring that the learned M focuses on them. Specifically, the adjacency matrix A is modified based on the pathway mask M as $A' = A \odot \sigma(M)$, where σ denotes the sigmoid function. Similarly, the features are masked as $X' = X \odot \sigma(M)$. The loss function for PathExplainer combines two components: a cross-entropy term for prediction consistency and regularization terms for sparsity:

$$\mathcal{L}_{\text{mask}} := -\sum_{c=1}^C 1[y=c] \log P_{\Phi}(Y=c | G=A', X=X')d + \lambda \|M\| \quad (10)$$

where $\|M\|$ encourages sparsity in the edge selection, and λ balances the trade-off between the classification loss and the sparsity regularization. Hence, the identified important subgraphs and node features (referring to AA sequence data) that contribute most to specific bio-networks can be considered as targeted pathways.

4 EXPERIMENTS AND RESULTS

Dataset and Preprocessing. We collected all available human pathway networks from the widely used knowledge database, KEGG [27]. Our dataset consists of four main classes: Human Diseases, Metabolism, Molecular and Cellular Processes, and Organismal Systems [26], covering 301 bio-networks. We searched for and downloaded all the raw data for the human pathway network (referred to as Homo sapiens) using KEGG APIs. To construct high-quality, trainable graphs, for nodes, we ensured that all protein nodes in the network were linked to their reference AA sequence data [29]. Protein nodes with a lack of or incomplete sequencing data were excluded. For edges, we streamlined the network structure by removing redundant or biologically insignificant interactions. We transformed preprocessed data into machine-learning-ready revision. The detailed data description and preprocessing pipeline can be found in Appendix C and Table 4.

Experimental Setup. We conducted 10-fold stratified K-Fold cross-validation repeated 5 times. The mean and standard deviation of the results across all folds were reported for evaluation. The hyperparameters were determined using grid search to identify the optimal configuration for the model. Training for all models was accomplished on NVIDIA A6000 GPU and Xeon Gold 6258R CPU.

4.1 Experiment-I: Pathway Representation

Objective. Evaluate the classification performance on unseen bio-networks, in line with Hypothesis-1, and benchmark the results against baseline models.

Baselines and Metrics. We collected baselines from both message-passing GNNs and more advanced graph models, including GCN [35], GraphSAGE [19], GAT [58], GIN [64], GPS [48], and GraphMamba [59]. The detailed introduction of these baselines and the selection motivation can be found in Appendix D. We used precision, recall, and overall accuracy for the performance evaluation. We used 650M ESM-2 for PathMamba and all baselines.

Results. Table 1 presents PathMamba achieves the highest accuracy (0.754), outperforming all GNNs, GPS (0.726), GraphMamba (0.723). Furthermore, it secures best or second-best positions across all functional categories, demonstrating its robust ability to generalize across diverse pathway structures. The superior performance of the proposed method highlights its effectiveness in extracting and leveraging biologically meaningful structural information from pathway networks. The gray-shaded rows indicate the results of removing ESM-2 and modifying the model size in terms of F1 scores. When ESM-2 is removed, the accuracy deteriorate significantly (0.75 \rightarrow 0.44), highlighting the importance of AA-seq and the limitations

Table 1: Baseline comparison results on bio-network classification. The best-performing and second-best results are highlighted in bold and underline, respectively. The gray-shaded rows indicate PathMamba (650M) with different ESM-2 parameter settings.

Methods	Human Diseases		Metabolism		Organismal Systems		Molecular & Cellular Processes		Overall Accuracy
	Precision	Recall	Precision	Recall	Precision	Recall	Precision	Recall	
GCN	0.632 ± 0.013	0.669 ± 0.022	0.895 ± 0.009	0.958 ± 0.007	0.644 ± 0.037	0.630 ± 0.023	0.570 ± 0.033	0.357 ± 0.025	0.683 ± 0.056
GraphSAGE	0.583 ± 0.020	0.633 ± 0.072	0.890 ± 0.007	0.959 ± 0.014	0.553 ± 0.041	0.575 ± 0.031	0.526 ± 0.059	0.337 ± 0.062	0.632 ± 0.037
GAT	0.630 ± 0.015	0.643 ± 0.036	0.932 ± 0.017	<u>0.970 ± 0.008</u>	<u>0.659 ± 0.015</u>	0.703 ± 0.010	0.560 ± 0.058	0.370 ± 0.025	0.690 ± 0.018
GIN	0.688 ± 0.023	0.697 ± 0.014	0.912 ± 0.016	0.944 ± 0.022	0.629 ± 0.025	0.638 ± 0.041	0.606 ± 0.032	<u>0.497 ± 0.027</u>	0.717 ± 0.013
GPS	<u>0.744 ± 0.018</u>	<u>0.729 ± 0.024</u>	0.893 ± 0.006	0.955 ± 0.014	0.634 ± 0.026	0.658 ± 0.011	0.629 ± 0.060	0.507 ± 0.019	<u>0.726 ± 0.014</u>
Graph-Mamba	0.707 ± 0.024	0.712 ± 0.024	0.897 ± 0.009	0.967 ± 0.007	0.626 ± 0.021	0.663 ± 0.033	0.700 ± 0.021	0.463 ± 0.032	0.723 ± 0.014
PathMamba	0.786 ± 0.029	0.800 ± 0.033	<u>0.915 ± 0.011</u>	0.972 ± 0.005	0.670 ± 0.026	0.703 ± 0.010	0.667 ± 0.035	<u>0.497 ± 0.028</u>	0.754 ± 0.015
w/ 3B	0.752 ± 0.022	0.726 ± 0.027	0.917 ± 0.008	0.973 ± 0.010	0.661 ± 0.017	0.663 ± 0.023	0.656 ± 0.032	0.550 ± 0.042	0.742 ± 0.009
w/ 150M	0.764 ± 0.031	0.764 ± 0.011	0.906 ± 0.011	0.975 ± 0.013	0.639 ± 0.023	0.688 ± 0.025	0.653 ± 0.029	0.510 ± 0.030	0.728 ± 0.013
w/ 35M	0.748 ± 0.033	0.751 ± 0.019	0.914 ± 0.005	0.969 ± 0.007	0.634 ± 0.028	0.663 ± 0.028	0.633 ± 0.055	0.510 ± 0.049	0.722 ± 0.013
w/o ESM-2	0.380 ± 0.008	0.585 ± 0.015	0.669 ± 0.015	0.585 ± 0.015	0.241 ± 0.007	0.063 ± 0.019	0.378 ± 0.030	0.377 ± 0.043	0.440 ± 0.010

Table 2: The computational efficiency comparison with hybrid models, including both training and inference runtime.

Methods	Training Time (msec)	Inference Time (msec)
GPS	29.2 ± 2.3	10.3 ± 0.3
Graph-Mamba	34.8 ± 0.4	9.5 ± 0.2
PathMamba	24.4 ± 0.9	6.9 ± 0.2

of prior studies that were unable to leverage this information. Increasing the model size gradually improves the results; however, accuracy does not incline with the 3B model (0.754 → 0.742). This suggests that excessively large features may lead to overfitting or noise, particularly in capturing functional pathways. Table 2 compares the training and inference times of our model with other expressive hybrid models, using a batch size of 32. Our training time is 30% faster than GPS and inference time is 27% faster than Graph-Mamba (complexity analysis can be found in Appendix B).

4.2 Experiment-II: Pathway Inference

Objective. Quantify the fidelity of extracted subgraphs, following our Hypothesis-2, and validate the importance of pathways specific to biological functions.

Baselines and Metrics. We collected baselines from conventional statistical methods (Random Sampling [34], PersonalizedPageRank [24], and MinimumDominatingSet [44, 63]), gradient-based methods (Saliency [52], InputXGradient [51], Deconvolution [42], ShapleyValueSampling [54], and GuidedBackpropagation [53]), and GNN-specific explainer methods (GNNExplainer [65] and PGExplainer [39]). All details can be found in Appendix D. We evaluated the distinctiveness of the pathways inferred by PathExplainer using fidelity metrics, specifically Fidelity+ and Fidelity-. Fidelity+ measures how well the important features identified by the model contribute to accurate predictions. In contrast, the fidelity- evaluates the drop in prediction accuracy when the identified important features are retained while others are removed. All details can be found in Appendix D and E.

Results. Figure 3 illustrates that PathExplainer achieves the highest fidelity+ and the lowest fidelity-, indicating its ability to explain necessary and sufficient subgraphs effectively. GNN-specific or

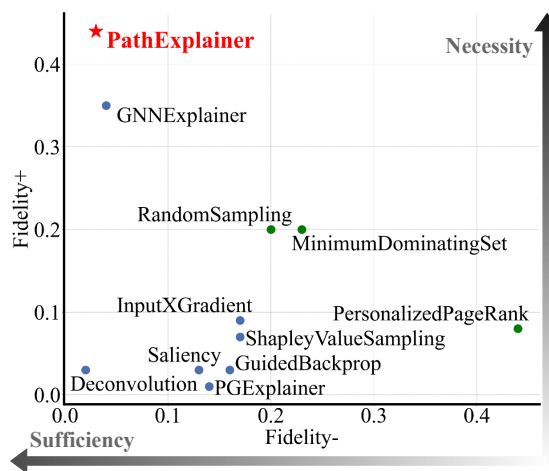


Figure 3: The fidelity+ (necessity ↑) and fidelity- (sufficiency ↓) scores of extracted subgraphs. Our PathExplainer achieves the best performance with the lowest fidelity+ and fidelity- scores, indicating its superior ability to produce robust and meaningful pathway networks.

gradient-based methods (blue points) show lower fidelity- compared to traditional methods (green points), demonstrating that the learned AA-seq enables the identification of sufficient subgraphs. PGExplainer exhibits lower fidelity+ than GNNExplainer, suggesting that instance-based approaches may be better suited for explaining diverse pathways.

4.3 Experiment-III: Biological Meaningfulness

Overview. We proposed an evaluation workflow to analyze the biological significance of the extracted subgraphs and pathways. This workflow directly integrates the weighting/ranking scores of pathway inferred by PathExplainer into biological metrics, enabling the direct quantification of outputs from deep learning models. Specifically, this includes: *Breadth*: The diversity of biological functions represented by the subgraphs. *Depth*: The extent to which gene nodes contribute to these biological functions. *Reliability*: The

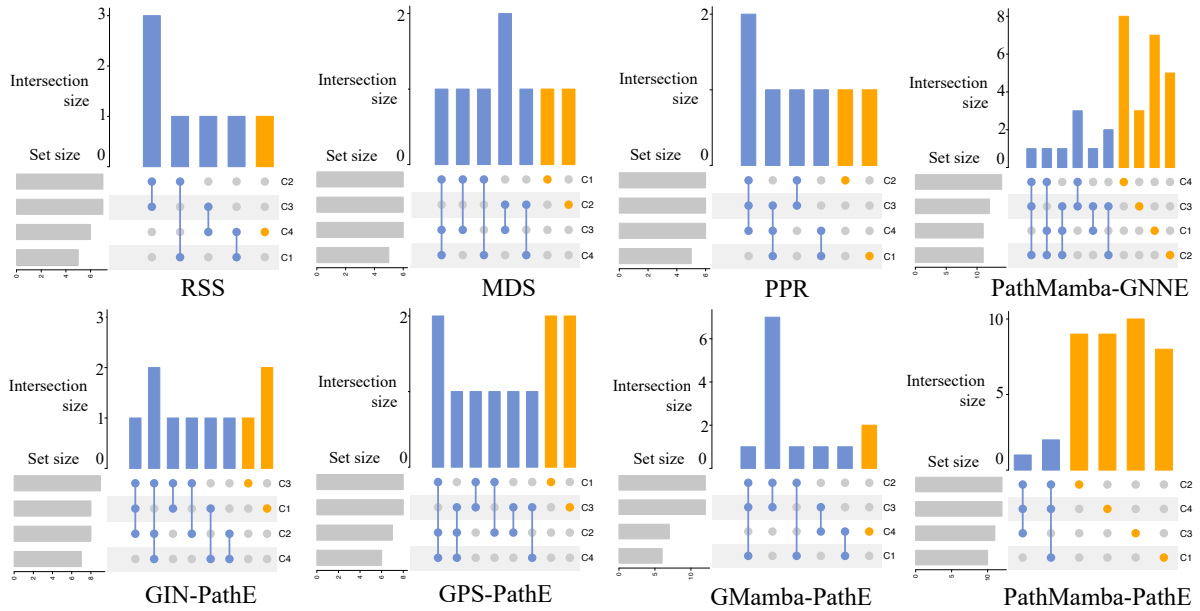


Figure 4: UpSet plot of enriched GO terms across four pathway classes, based on top feature sets from subgraphs for different methods. Orange indicates GO terms uniquely enriched in one class, and blue represents GO terms shared across multiple classes. RSS, MDS, and PPR stand for Random Sampling, Minimum Dominating Set, and Personalized PageRank, respectively.

robustness and statistical significance of the analyses targeting these biological functions.

Setup and Metrics. To this end, we designed experiments centered on Gene Ontology (GO) analysis [4], focusing on the nodes within the extracted subgraphs. The results provide a list of GO terms highlighting the biological functions most significantly represented in the input gene (corresponding to protein) nodes [4]. *Breadth* was assessed using the Number of Enriched Biological Functions (**#EBF**). A higher #EBF indicates broader functional diversity within the subgraph. *Depth* was evaluated using a new metric called the Enrichment Contribution Score (**ECS**). ECS evaluates the relative contribution of the top-weighted genes, denoted as G_{Top} . Here we directly framed the inferred pathways as the targets of ECS to generate G_{Top} for evaluations by following steps: Let $G = \{g_1, g_2, \dots, g_n\}$ represent the ranked list of gene nodes, sorted by the importance weights of pathways (inferred directly by PathExplainer) $w = \{w_1, w_2, \dots, w_n\}$, where $w_1 \geq w_2 \geq \dots \geq w_n$. Define $G_{\text{Top}} = \{g_1, g_2, \dots, g_{\text{Top}}\}$ to include only genes with the top weights, selected based on a ratio $R\%$ (defaulted as 30%), as a subset of G . Then, perform GO analysis based on G_{Top} for each input subgraph S_i . The ECS is calculated as the average number of enriched items for each gene in G_{Top} across all subgraphs S_i , and is defined as:

$$\text{ECS} = \frac{1}{P} \sum_{i=1}^P \frac{|GO_{\text{top-enriched}}(S_i)|}{|G_{\text{Top}}|},$$

where P is the total number of tested subgraphs, $GO_{\text{top-enriched}}(S_i)$ is the set of enriched GO terms for subgraph S_i based on G_{Top} , and $|G_{\text{Top}}|$ is the number of genes in the subset G_{Top} . Moreover,

Table 3: Biological meaningfulness comparison results on subgraphs extracted by different methods. The best-performing results are highlighted in bold. The second-best results are highlighted in underline.

Methods	#EBF (\uparrow)	ECS (\uparrow)	P-value (\downarrow)
RSS	5.29	0.27	0.045
MDS	6.34	0.23	0.043
PPR	6.64	0.23	0.042
GIN-GNNE	6.94	0.59	0.041
GPS-GNNE	8.88	0.22	0.039
GMamba-GNNE	10.73	0.21	0.042
PathMamba-GNNE	<u>11.89</u>	<u>0.73</u>	0.036
GIN-PathE	11.06	0.69	0.041
GPS-PathE	8.26	0.43	<u>0.037</u>
GMamba-PathE	10.89	0.59	0.038
ExPath	14.77	0.84	0.036

Reliability assessed using **P-value**. We accepted the item only with a P-value lower than 0.05, the average P-value reported here is naturally lower than this threshold. A lower average indicates greater reliability in the enrichment results across the subgraphs. The details of GO and metrics can be found in Appendix E.

Results. Table 3 presents the biological meaningfulness comparison results for subgraphs extracted using different methods. Overall, PathMamba-PathE achieves the highest performance across #EBF, ECS, and P-value. This highlights its ability to extract biologically

relevant structures within pathway networks, effectively balancing breadth and depth. While conventional methods (RSS, MDS, and PPR) perform relatively poorly in overall #EBF and ECS, with almost boundary P-values achieved.

Figure 4 evaluates the differences in enriched GO terms across four pathway classes based on top gene sets from subgraphs extracted by different methods. Compared with other methods, the upset plot reveals that PathMamba-PathE identifies the most extensive sets of unique GO terms (shown as the orange bars and links) across all four pathway classes while maintaining fewer shared terms (shown as the blue bars and links) among different classes. This suggests that PathMamba-PathE tends to assign appropriate weights to genes based on their importance within the network and effectively captures the distinct biological roles of top-ranked genes in specific pathway classes.

4.4 Case Study: T Cell Receptor Signaling Pathway Evaluation

Setup. The T cell receptor (TCR) signaling pathway is a classic example of well-characterized human pathways. It would be helpful if parts implying key aberrations could be found as sub-graphs in the whole pathway graph. In this case study, we compare subgraphs extracted by two methods: TCR Subgraph A, generated using the RSS method, and Subgraph B, obtained via our proposed method. Each method selects the top 10% highest-ranked nodes and their associated edges to construct a representative subgraph. The detailed information and results analysis of the case study can be found in Appendix G.

TCR Subgraph A: The RSS Method. As shown in Figure 5, subgraph A, generated by the RSS method, distributes high scores uniformly across a broad range of nodes within the TCR pathway. However, this hints at unnatural, fragmented signal propagation, as highlighted by numerous discrete red-marked nodes.

TCR Subgraph B: The Proposed Method. In contrast, as shown in Figure 5 subgraph B, the subgraph extracted by our method exhibits a strong focus on the PI3K-AKT signaling axis [57] and the downstream components of the NF- κ B [12] pathway, as highlighted by the coherent red-marked path.

Discuss. In summary, the proposed method’s subgraphs align with real-world pathway analysis practices’ needs: maintaining **signal continuity within regulatory cascades** and even holding relatively long signaling paths, making it more suitable for focused analyses of bio-network regulatory mechanisms.

5 RELATED WORK

Existing methods for analyzing the structure of biological networks typically represent these networks as graphs, aiming to infer sub-graphs or extract relevant interactions, and can generally be categorized into statistical topology-driven and data-driven deep graph learning methods.

Topology-driven methods utilize statistical metrics on structural properties of graphs, such as node degrees [31, 33], centrality [20, 44, 60], betweenness, or PageRank scores [24, 41] to infer which substructures or edges exert a more significant influence on the overall topology, thereby identifying more targeted interactions among genes or proteins.

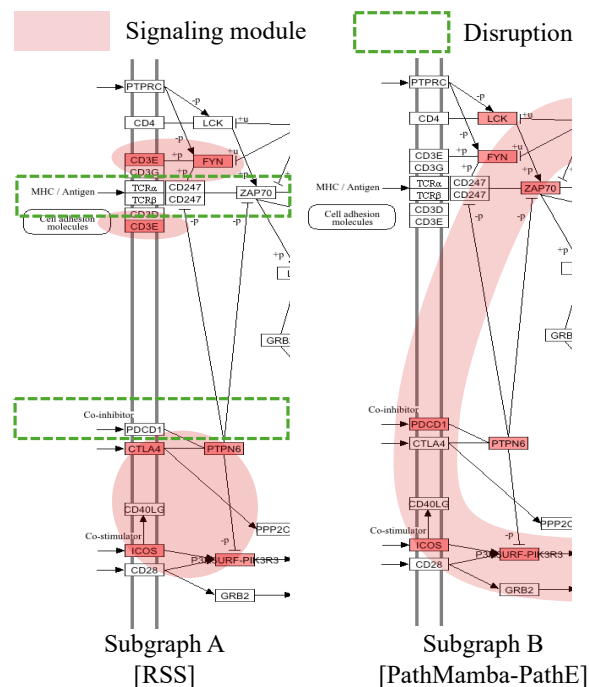


Figure 5: Comparison of subgraphs extracted from the TCR signaling pathway using two different methods. TCR Subgraph A is from the RSS method, and TCR Subgraph B is from the proposed method. The subgraph nodes and their signaling modules are colored in red. The disruptions within signaling paths are marked in green boxes.

Deep graph learning methods incorporate experimental data during the learning process by embedding data as node representations. They train graph neural networks (GNNs) with suitable objectives, such as link prediction or graph reconstruction [43, 67, 70], and the links that contribute most to these objectives can be considered the targeted interactions. For instance, the classic GCN algorithm, GraphSAGE [19], has been validated on protein-protein interaction (PPI) datasets to predict protein functions within networks. The work of [17] introduced a GCN-based method for predicting protein functions, leveraging sequence features derived from a protein language model alongside structural information. Chen et al. [11] employed a graph attention network to extract drug and protein AA-Seq features for predicting drug-target interactions. Moreover, GNN models have been applied to incorporate RNA-Seq data, for tasks like predicting disease states and cell-cell relationships [49, 61].

6 CONCLUSION

We introduced ExPath, a novel framework for understanding targeted pathways within biological database. ExPath integrates (1) a protein language model (pLM) for encoding AA-seqs into graph features, (2) PathMamba, a hybrid model to capture local and global dependencies, and (3) PathExplainer, a subgraph learning module that identifies key nodes and edges via trainable pathway masks. We also introduced ML-oriented biological evaluations and a new

metric. The experiments involving 301 bio-networks evaluations demonstrated that pathways inferred by ExPath maintain biological meaningfulness. We will release all code and curated 301 bio-network data to facilitate reproducibility and enable future research in data-specific bio-network inference. Future work will expand ExPath to analyze other types of bio-networks, enabling broader applications in systems biology and medicine.

REFERENCES

- [1] Eric Alm and Adam P Arkin. 2003. Biological networks. *Current opinion in structural biology* 13, 2 (2003), 193–202.
- [2] Stephen F Altschul, Thomas L Madden, Alejandro A Schäffer, Jinghui Zhang, Zheng Zhang, Webb Miller, and David J Lipman. 1997. Gapped BLAST and PSI-BLAST: a new generation of protein database search programs. *Nucleic acids research* 25, 17 (1997), 3389–3402.
- [3] Kiyoko F Aoki and Minoru Kanehisa. 2005. Using the KEGG database resource. *Current protocols in bioinformatics* 11, 1 (2005), 1–12.
- [4] Michael Ashburner, Catherine A Ball, Judith A Blake, David Botstein, Heather Butler, J Michael Cherry, Allan P Davis, Kara Dolinski, Selina S Dwight, Janan T Eppig, et al. 2000. Gene ontology: tool for the unification of biology. *Nature genetics* 25, 1 (2000), 25–29.
- [5] Albert-László Barabási, Natali Gulbahce, and Joseph Loscalzo. 2011. Network medicine: a network-based approach to human disease. *Nature reviews genetics* 12, 1 (2011), 56–68.
- [6] Albert-Laszlo Barabasi and Zoltan N Oltvai. 2004. Network biology: understanding the cell’s functional organization. *Nature reviews genetics* 5, 2 (2004), 101–113.
- [7] Ali Behrouz and Farnoosh Hashemi. 2024. Graph Mamba: Towards Learning on Graphs with State Space Models. In *Proceedings of the 30th ACM SIGKDD Conference on Knowledge Discovery and Data Mining (KDD ’24)*. 119–130.
- [8] Stefan Bornholdt. 2005. Less is more in modeling large genetic networks. *Science* 310, 5747 (2005), 449–451.
- [9] Tyrell Cartwright, Neil D Perkins, and Caroline L. Wilson. 2016. NFKB1: a suppressor of inflammation, ageing and cancer. *The FEBS journal* 283, 10 (2016), 1812–1822.
- [10] Jiezhong Chen, Ross Crawford, and Yin Xiao. 2013. Vertical inhibition of the PI3K/Akt/mTOR pathway for the treatment of osteoarthritis. *Journal of cellular biochemistry* 114, 2 (2013), 245–249.
- [11] Zhongjian Cheng, Cheng Yan, Fang-Xiang Wu, and Jianxin Wang. 2021. Drug-target interaction prediction using multi-head self-attention and graph attention network. *IEEE/ACM Transactions on Computational Biology and Bioinformatics* 19, 4 (2021), 2208–2218.
- [12] Xavier Dolcet, David Llobet, Judit Pallares, and Xavier Matias-Guiu. 2005. NF- κ B in development and progression of human cancer. *Virchows archiv* 446 (2005), 475–482.
- [13] Warren N D’Souza, Chiung-Fang Chang, April M Fischer, Manqing Li, and Stephen M Hedrick. 2008. The Erk2 MAPK regulates CD8 T cell proliferation and survival. *The Journal of Immunology* 181, 11 (2008), 7617–7629.
- [14] Vijay Prakash Dwivedi, Anh Tuan Luu, Thomas Laurent, Yoshua Bengio, and Xavier Bresson. 2022. Graph Neural Networks with Learnable Structural and Positional Representations. In *International Conference on Learning Representations*.
- [15] Robert D Finn, Alex Bateman, Jody Clements, Penelope Coghill, Ruth Y Eberhardt, Sean R Eddy, Andreas Heger, Kirstie Hetherington, Liisa Holm, Jaina Mistry, et al. 2014. Pfam: the protein families database. *Nucleic acids research* 42, D1 (2014), D222–D230.
- [16] Guillaume Gaud, Renaud Lesourne, and Paul E Love. 2018. Regulatory mechanisms in T cell receptor signalling. *Nature Reviews Immunology* 18, 8 (2018), 485–497.
- [17] Vladimir Gligorijević, P Douglas Renfrew, Tomasz Kosciolc, Julia Koehler Leman, Daniel Berenberg, Tommi Vatanen, Chris Chandler, Bryn C Taylor, Ian M Fisk, Hera Vlamakis, et al. 2021. Structure-based protein function prediction using graph convolutional networks. *Nature communications* 12, 1 (2021), 3168.
- [18] Albert Gu and Tri Dao. 2024. Mamba: Linear-Time Sequence Modeling with Selective State Spaces. *arXiv preprint arXiv:2312.00752* (2024). arXiv:2312.00752
- [19] Will Hamilton, Zhitao Ying, and Jure Leskovec. 2017. Inductive Representation Learning on Large Graphs. In *Advances in Neural Information Processing Systems*.
- [20] Teresa W Haynes, Stephen Hedetniemi, and Peter Slater. 2013. *Fundamentals of domination in graphs*. CRC press.
- [21] Da Wei Huang, Brad T Sherman, and Richard A Lempicki. 2009. Bioinformatics enrichment tools: paths toward the comprehensive functional analysis of large gene lists. *Nucleic acids research* 37, 1 (2009), 1–13.
- [22] Morgan Huse. 2009. The T-cell-receptor signaling network. *Journal of cell science* 122, 9 (2009), 1269–1273.
- [23] Trey Ideker and Nevan J Krogan. 2012. Differential network biology. *Molecular systems biology* 8, 1 (2012), 565.
- [24] Gábor Iván and Vince Grolmusz. 2011. When the Web meets the cell: using personalized PageRank for analyzing protein interaction networks. *Bioinformatics (Oxford, England)* (2011), 405–407.
- [25] John Jumper, Richard Evans, Alexander Pritzel, Tim Green, Michael Figurnov, Olaf Ronneberger, Kathryn Tunyasuvunakool, Russ Bates, Augustin Židek, Anna Potapenko, et al. 2021. Highly accurate protein structure prediction with AlphaFold. *nature* 596, 7873 (2021), 583–589.
- [26] Minoru Kanehisa, Miho Furumichi, Yoko Sato, Yuriko Matsuura, and Mari Ishiguro-Watanabe. 2024. KEGG: biological systems database as a model of the real world. *Nucleic Acids Research* (2024), D672–D677.
- [27] Minoru Kanehisa and Susumu Goto. 2000. KEGG: kyoto encyclopedia of genes and genomes. *Nucleic acids research* 28, 1 (2000), 27–30.
- [28] Minoru Kanehisa and Yoko Sato. 2020. KEGG Mapper for inferring cellular functions from protein sequences. *Protein Science* 29, 1 (2020), 28–35.
- [29] Minoru Kanehisa, Yoko Sato, Masayuki Kawashima, Miho Furumichi, and Mao Tanabe. 2016. KEGG as a reference resource for gene and protein annotation. *Nucleic acids research* 44, D1 (2016), D457–D462.
- [30] Chuanze Kang, Han Zhang, Zhuo Liu, Shenwei Huang, and Yanbin Yin. 2022. LR-GNN: A graph neural network based on link representation for predicting molecular associations. *Briefings in Bioinformatics* 23, 1 (2022), bbab513.
- [31] David R Karger. 1994. Random sampling in cut, flow, and network design problems. In *Proceedings of the twenty-sixth annual ACM symposium on Theory of computing*. 648–657.
- [32] Guy Karlebach and Ron Shamir. 2008. Modelling and analysis of gene regulatory networks. *Nature reviews Molecular cell biology* 9, 10 (2008), 770–780.
- [33] Nadav Kashtan, Shalev Itzkovitz, Ron Milo, and Uri Alon. 2004. Efficient sampling algorithm for estimating subgraph concentrations and detecting network motifs. *Bioinformatics* 20, 11 (2004), 1746–1758.
- [34] N. Kashtan, S. Itzkovitz, R. Milo, and U. Alon. 2004. Efficient sampling algorithm for estimating subgraph concentrations and detecting network motifs. *Bioinformatics* (2004), 1746–1758.
- [35] Thomas N. Kipf and Max Welling. 2017. Semi-Supervised Classification with Graph Convolutional Networks. In *International Conference on Learning Representations*.
- [36] Menglu Li, Zhiwei Wang, Luotao Liu, Xuan Liu, and Wen Zhang. 2024. Subgraph-Aware Graph Kernel Neural Network for Link Prediction in Biological Networks. *IEEE Journal of Biomedical and Health Informatics* (2024).
- [37] Rong Li, Yu Li, Xiao Liang, Lu Yang, Min Su, and Keng Po Lai. 2021. Network Pharmacology and bioinformatics analyses identify intersection genes of niacin and COVID-19 as potential therapeutic targets. *Briefings in Bioinformatics* 22, 2 (2021), 1279–1290.
- [38] Zeming Lin, Halil Akin, Roshan Rao, Brian Hie, Zhongkai Zhu, Wenting Lu, Nikita Smetanin, Robert Verkuil, Ori Kabeli, Yaniv Shmueli, et al. 2023. Evolutionary-scale prediction of atomic-level protein structure with a language model. *Science* (2023), 1123–1130.
- [39] Dongsheng Luo, Wei Cheng, Dongkuan Xu, Wenchao Yu, Bo Zong, Haifeng Chen, and Xiang Zhang. 2020. Parameterized Explainer for Graph Neural Network. In *Advances in Neural Information Processing Systems*. 19620–19631.
- [40] Thomas Madden. 2013. The BLAST sequence analysis tool. *The NCBI handbook* 2, 5 (2013), 425–436.
- [41] Takanori Maehara, Takuya Akiba, Yoichi Iwata, and Ken-ichi Kawarabayashi. 2014. Computing personalized pagerank quickly by exploiting graph structures. *Proceedings of the VLDB Endowment* 7, 12 (2014), 1023–1034.
- [42] Aravindh Mahendran and Andrea Vedaldi. 2016. Salient deconvolutional networks. In *ECCV 2016: 14th European Conference, Amsterdam, The Netherlands, October 11–14, 2016, Proceedings, Part VI* 14. 120–135.
- [43] Giulia Muzio, Leslie O’Bray, and Karsten Borgwardt. 2021. Biological network analysis with deep learning. *Briefings in bioinformatics* 22, 2 (2021), 1515–1530.
- [44] Jose C. Nacher and Tatsuya Akutsu. 2016. Minimum dominating set-based methods for analyzing biological networks. *Methods* 102 (2016), 57–63.
- [45] Georgios A Pavlopoulos, Maria Secrier, Charalampos N Moschopoulos, Theodoros G Soldatos, Sophia Kossida, Jan Aerts, Reinhard Schneider, and Pantelis G Bagos. 2011. Using graph theory to analyze biological networks. *BioData mining* 4 (2011), 1–27.
- [46] Eric M Phizicky and Stanley Fields. 1995. Protein-protein interactions: methods for detection and analysis. *Microbiological reviews* 59, 1 (1995), 94–123.
- [47] Sarwish Rafiq, Christopher S Hackett, and Renier J Brentjens. 2020. Engineering strategies to overcome the current roadblocks in CAR T cell therapy. *Nature reviews Clinical oncology* 17, 3 (2020), 147–167.
- [48] Ladislav Rampásek, Michael Galkin, Vijay Prakash Dwivedi, Anh Tuan Luu, Guy Wolf, and Dominique Beaini. 2022. Recipe for a General, Powerful, Scalable Graph Transformer. In *Advances in Neural Information Processing Systems*. 14501–14515.

- [49] Neal Ravindra, Arijit Sehanobish, Jenna L Pappalardo, David A Hafler, and David van Dijk. 2020. Disease state prediction from single-cell data using graph attention networks. In *Proceedings of the ACM conference on health, inference, and learning*. 121–130.
- [50] Kinjal Shah, Amr Al-Haidari, Jianmin Sun, and Julhash U Kazi. 2021. T cell receptor (TCR) signaling in health and disease. *Signal transduction and targeted therapy* 6, 1 (2021), 412.
- [51] Avanti Shrikumar, Peyton Greenside, and Anshul Kundaje. 2017. Learning important features through propagating activation differences. In *Proceedings of the 34th International Conference on Machine Learning (ICML '17)*. 3145–3153.
- [52] Karen Simonyan, Andrea Vedaldi, and Andrew Zisserman. 2013. Deep inside convolutional networks: Visualising image classification models and saliency maps. *arXiv preprint arXiv:1312.6034* (2013).
- [53] Jost Tobias Springenberg, Alexey Dosovitskiy, Thomas Brox, and Martin Riedemiller. 2014. Striving for simplicity: The all convolutional net. *arXiv preprint arXiv:1412.6806* (2014).
- [54] Erik Strumbelj and Igor Kononenko. 2010. An Efficient Explanation of Individual Classifications using Game Theory. *J. Mach. Learn. Res.* (2010), 1–18.
- [55] Damian Szklarczyk, Rebecca Kirsch, Mikaela Koutrouli, Katerina Nastou, Farrokh Mehryary, Radja Hachilif, Annika L Gable, Tao Fang, Nadezhda T Doncheva, Sampo Pyysalo, et al. 2023. The STRING database in 2023: protein–protein association networks and functional enrichment analyses for any sequenced genome of interest. *Nucleic acids research* 51, D1 (2023), D638–D646.
- [56] Jan Tonshoff, Martin Ritzert, Hinrikus Wolf, and Martin Grohe. 2023. Walking Out of the Weisfeiler Leman Hierarchy: Graph Learning Beyond Message Passing. *Transactions on Machine Learning Research* (2023).
- [57] Juan Ángel Fresno Vara, Enrique Casado, Javier de Castro, Paloma Cejas, Cristóbal Belda-Iniesta, and Manuel González-Barón. 2004. PI3K/Akt signalling pathway and cancer. *Cancer treatment reviews* 30, 2 (2004), 193–204.
- [58] Petar Veličković, Guillem Cucurull, Arantxa Casanova, Adriana Romero, Pietro Liò, and Yoshua Bengio. 2018. Graph Attention Networks. In *International Conference on Learning Representations*.
- [59] Chloe Wang, Oleksii Tsepa, Jun Ma, and Bo Wang. 2024. Graph-Mamba: Towards Long-Range Graph Sequence Modeling with Selective State Spaces. *arXiv preprint arXiv:2402.00789* (2024). arXiv:2402.00789
- [60] Haiying Wang, Huiru Zheng, Fiona Browne, and Chaoyang Wang. 2014. Minimum dominating sets in cell cycle specific protein interaction networks. In *2014 IEEE International Conference on Bioinformatics and Biomedicine (BIBM)*. IEEE, 25–30.
- [61] Juexin Wang, Anjun Ma, Yuzhou Chang, Jianting Gong, Yuexu Jiang, Ren Qi, Cankun Wang, Hongjun Fu, Qin Ma, and Dong Xu. 2021. scGNN is a novel graph neural network framework for single-cell RNA-Seq analyses. *Nature communications* 12, 1 (2021), 1882.
- [62] Qing-Wen Wu, Jun-Feng Xia, Jian-Cheng Ni, and Chun-Hou Zheng. 2021. GAERF: predicting lncRNA-disease associations by graph auto-encoder and random forest. *Briefings in bioinformatics* 22, 5 (2021), bbaa391.
- [63] Stefan Wuchty. 2014. Controllability in protein interaction networks. *Proceedings of the National Academy of Sciences* (2014), 7156–7160.
- [64] Keyulu Xu, Weihua Hu, Jure Leskovec, and Stefanie Jegelka. 2019. How Powerful are Graph Neural Networks?. In *International Conference on Learning Representations*.
- [65] Zhitao Ying, Dylan Bourgeois, Jiaxuan You, Marinka Zitnik, and Jure Leskovec. 2019. GNNExplainer: Generating Explanations for Graph Neural Networks. In *Advances in Neural Information Processing Systems*.
- [66] Guangchuan Yu, Li-Gen Wang, Yanyan Han, and Qing-Yu He. 2012. clusterProfiler: an R package for comparing biological themes among gene clusters. *Omic: a journal of integrative biology* 16, 5 (2012), 284–287.
- [67] Xiang Yue, Zhen Wang, Jingong Huang, Srinivasan Parthasarathy, Soheil Moosavinasab, Yungui Huang, Simon M Lin, Wen Zhang, Ping Zhang, and Huan Sun. 2020. Graph embedding on biomedical networks: methods, applications and evaluations. *Bioinformatics* 36, 4 (2020), 1241–1251.
- [68] Naif Zaman, Lei Li, Maria Luz Jaramillo, Zhanpeng Sun, Chabane Tibiche, Myriam Banville, Catherine Collins, Mark Trifiro, Miltiadis Paliouras, Andre Nantel, et al. 2013. Signaling network assessment of mutations and copy number variations predict breast cancer subtype-specific drug targets. *Cell reports* (2013), 216–223.
- [69] Wen Zhang, Yanlin Chen, Feng Liu, Fei Luo, Gang Tian, and Xiaohong Li. 2017. Predicting potential drug-drug interactions by integrating chemical, biological, phenotypic and network data. *BMC bioinformatics* 18 (2017), 1–12.
- [70] Xiao-Meng Zhang, Li Liang, Lin Liu, and Ming-Jing Tang. 2021. Graph neural networks and their current applications in bioinformatics. *Frontiers in genetics* 12 (2021), 690049.
- [71] Chengshuai Zhao, Shuai Liu, Feng Huang, Shichao Liu, and Wen Zhang. 2021. CSGNN: Contrastive Self-Supervised Graph Neural Network for Molecular Interaction Prediction.. In *IJCAL*. 3756–3763.
- [72] Marinka Zitnik, Michelle M Li, Aydin Wells, Kimberly Glass, Deisy Morselli Gysi, Arjun Krishnan, T M Murali, Predrag Radivojac, Sushmita Roy, Anaïs Baudot, Serdar Bozdag, Danny Z Chen, Lenore Cowen, Kapil Devkota, Anthony Gitter, Sara J C Gosline, Pengfei Gu, Pietro H Guzzi, Heng Huang, Meng Jiang, Ziyinet Nesibe Kesimoglu, Mehmet Koyuturk, Jian Ma, Alexander R Pico, Nataša Pržulj, Teresa M Przytycka, Benjamin J Raphael, Anna Ritz, Roded Sharan, Yang Shen, Mona Singh, Donna K Slonim, Hanghang Tong, Xinan Holly Yang, Byung-Jun Yoon, Haiyuan Yu, and Tijana Milenković. 2024. Current and future directions in network biology. *Bioinformatics Advances* (2024), vbae099.

APPENDIX

Table 4: Summary of pathway data across four pathway classes.

Pathway class	#Samples	#Nodes	#Edges	AA-seq Length
C1 Human Diseases	83	40	42	583
C2 Metabolism	78	16	42	511
C3 Molecular and cellular processes	80	30	37	636
C4 Organismal systems	60	44	49	638
Overall	301	32	42	590

A GRAPH ISOMORPHISM AND WL TEST

Graph isomorphism refers to the problem of determining whether two graphs are structurally identical, meaning there exists a one-to-one correspondence between their nodes and edges. This is a crucial challenge in graph classification tasks, where the goal is to assign labels to entire graphs based on their structures. A model that can effectively differentiate non-isomorphic graphs is said to have high expressiveness, which is essential for accurate classification. In many cases, graph classification models like GNNs rely on graph isomorphism tests to ensure that structurally distinct graphs receive different embeddings, which improves the model’s ability to correctly classify graphs.

Weisfeiler-Lehman (WL) test is a widely used graph isomorphism test that forms the foundation of many GNNs. In the 1-WL framework, each node’s representation is iteratively updated by aggregating information from its neighboring nodes, followed by a hashing process to capture the structural patterns of the graph. GNNs leveraging this concept, such as Graph Convolutional Networks (GCNs) and Graph Attention Networks (GATs), essentially perform a similar neighborhood aggregation, making them as expressive as the 1-WL test in distinguishing non-isomorphic graphs [64]. Modern GNN architectures adhere to this paradigm, making the 1-WL a standard baseline for GNN expressivity.

A.1 Theoretical Analysis

We analyze our explained pathways based on the Weisfeiler-Lehman (WL) tests and expressiveness.

Lemma 1. (*Expressiveness for explanations*). *When combined with higher expressive models (e.g., it distinguishes more graphs), PathExplainer can generate more finely differentiated (and potentially more “faithful”) explanation pathways (subgraphs). In contrast, a less expressive model merges different graphs (or nodes/substructures) into larger equivalence classes, leading to non-unique, less granular explanations.*

PROOF. Let $f : \mathcal{G} \rightarrow \mathbb{R}^k$ be a GNN-based model, and let \sim denote the equivalence relation induced by f , i.e.,

$$G \sim H \iff f(G) = f(H).$$

Consider a GNNExplainer objective given by

$$\mathcal{L}(E; f, G) = \alpha \cdot D(f(G), f(G \setminus E)) + \beta \cdot \Omega(E),$$

where $E \subseteq \text{components}(G)$ (e.g., a subset of edges/nodes/features), $D(\cdot, \cdot)$ is a distance or divergence measure between outputs, and

$\Omega(E)$ is a regularization term encouraging compactness or sparsity. Define the explainer’s solution by

$$E^*(G) = \operatorname{argmin}_{E \subseteq G} \mathcal{L}(E; f, G).$$

If $G \sim H$, then any pair of optimal explanations $E^*(G)$ and $E^*(H)$ must yield the same minimum objective value. Consequently, there is no unique explanation across G and H within the same equivalence class.

Since $G \sim H$, we have $f(G) = f(H)$. By definition of $E^*(G)$,

$$\mathcal{L}(E^*(G); f, G) = \min_{E \subseteq G} \mathcal{L}(E; f, G).$$

Similarly, for H ,

$$\mathcal{L}(E^*(H); f, H) = \min_{E \subseteq H} \mathcal{L}(E; f, H).$$

Because $f(G) = f(H)$, the distance term $D(f(G), f(G \setminus E))$ behaves the same as $D(f(H), f(H \setminus E))$ for corresponding substructures E (insofar as the GNN does not distinguish between the same substructure in G and that in H). Furthermore, if G and H are isomorphic under the viewpoint of f , any subgraph E_G of G can be mapped to a subgraph E_H of H with equivalent contribution to $D(\cdot, \cdot)$ and to $\Omega(\cdot)$.

Hence, there exists a subgraph $E_H \subseteq H$ such that

$$\mathcal{L}(E_H; f, H) = \mathcal{L}(E^*(G); f, G).$$

Likewise, one can construct a subgraph E_G from $E^*(H)$ with the same objective value. Thus, for any $G \sim H$,

$$\mathcal{L}(E^*(G); f, G) = \mathcal{L}(E^*(H); f, H),$$

which implies the optimal explanations are not uniquely determined beyond the equivalence class $[G]$ (the set of all graphs equivalent to G). In other words, the GNNExplainer’s solution within an equivalence class \sim cannot uniquely distinguish between graphs G and H such that $G \sim H$. Less expressive models merges different graphs (or nodes/substructures) into larger equivalence classes, leading to non-unique, less granular explanations. In contrast, PathExplainer can generate more finely differentiated explanation subgraphs, when combined with higher expressive models. \square

Lemma 2 (Comparison with k -WL test). *For every $k \geq 1$ there are graphs that are distinguishable by PathMamba, but not by k -WL (and hence not by k -WL GNNs).*

PROOF. The proof of this theorem directly comes from the recent work [7, 56]. They prove a similar theorem using 1-d CNN [56] or SSM [7] with random sampled subgraph. \square

Lemma 3 (Comparison with 1-WL test). *PathMamba is strictly more expressive than 1-WL GNNs.*

PROOF. We first note that PathMamba contains the GIN as a submodule, which has the same expressive power as the 1-WL test [64]. Therefore, PathMamba is at least as expressive as 1-WL GNNs. By Lemma 2, there are graphs that cannot be distinguished by 1-WL GNNs, but can be distinguished by PathMamba. Consequently, PathMamba is strictly more expressive than 1-WL GNNs. \square

Theorem 1 (Explanations of ExPath). *Based on Lemma 1, 2, and 3, ExPath can generate more finely differentiated (and potentially more “faithful”) explanation pathways (subgraphs) than 1-WL GNN-based methods, and not bounded by any WL GNN methods.*

B COMPUTATIONAL COMPLEXITY ANALYSIS

Given K tokens, the complexity of Mamba [18] is linear with respect to K . For $m \geq 1$, for each node $v \in V$, we generate $|V|$ sampled pathways with length m , the time complexity of global module mamba would be:

$$O(|V| \times m),$$

since we have $O(|V| \times m)$ tokens. Our PathMamba is faster than the quadratic time complexity $O(|V|^2)$ of graph transformers [48].

In practice, combined with GNN, which requires $O(|V| + |E|)$ time, the total complexity would be:

$$O(|V| + |E|),$$

dominated by the GNN complexity, since m represents only a subset of pathways sampled from the total possible nodes V ($m \ll |V|$).

C PREPROCESSING

The KEGG database is a comprehensive resource that integrates genomic, chemical, and systemic functional information, providing curated pathway networks for various biological processes derived from experimental data and expert annotations. For human pathways, KEGG offers detailed representations of processes such as metabolism, genetic information processing, environmental information processing, and human diseases. Each category includes pathways organized into networks, where nodes represent biological entities—such as genes, proteins, enzymes, or metabolites—and edges denote their interactions. These interactions encompass direct biochemical reactions, regulatory relationships, and signaling pathways that govern cellular mechanisms, ultimately forming pathways related to various functional biological processes.

We searched for and downloaded all the raw data for the human pathway network (referred to as Homo Sapiens in most bio-databases) using KEGG APIs. The data underwent a series of preprocessing steps to ensure its quality and relevance. (1) First, we ensured that all protein nodes in the network were linked to well-characterized genetic origins, specifically their reference amino acid sequence data [29]. Using KEGG’s gene-to-protein mapping, we filtered the dataset to retain only protein nodes with associated genomic annotations [28]. Protein nodes lacking sequencing data or genetic associations in KEGG were excluded to reduce noise caused by incomplete or ambiguous sequence information. For the retained nodes, their amino acid sequences were extracted and utilized as input features, ensuring a biologically meaningful representation for the learning task. (2) Second, we streamlined the network structure by removing redundant or biologically insignificant interactions. Specifically, we eliminated non-functional self-loops (edges connecting a node to itself without annotated biological relevance) and isolated nodes lacking any edges. This process included both nodes that were initially isolated and those rendered isolated following the first step of node filtering. Since these elements no longer contributed to the network’s connectivity or functional variation, their removal reduced unnecessary complexity and ensured the

network focused exclusively on meaningful and biologically interpretable interactions [8]. (3) Third, we preserved the edge with properties of protein-protein interactions while removing directional information to transform the network into an undirected graph. This conversion enabled the analysis to emphasize undirected, pairwise interactions, which are often more pertinent to network-based studies, such as clustering, community detection, or functional enrichment analyses. (4) Finally, the pathways were organized into functional classes based on their KEGG pathway labels, ensuring that biologically related pathways were grouped together. The original labels for Environmental Information Processing and Genetic Information Processing were combined into a unified class, Molecular and Cellular Processes, to reflect their shared biological roles in cellular signaling, communication, and gene regulation [3]. As a result, the pathway data used in this study was categorized into four main classes: Human Diseases, Metabolism, Molecular and Cellular Processes, and Organismal Systems.

D BASELINE

We collected baselines from both message-passing GNNs and more advanced graph models. Graph Convolutional Network (GCN) [35] serves as a foundational GNN, leveraging spectral graph theory for node feature aggregation. GraphSAGE [19] improves scalability by introducing neighborhood sampling and learnable aggregation functions. Graph Attention Network (GAT) [58] incorporates attention mechanisms to assign different importance to neighbors during feature aggregation. Graph Isomorphism Network (GIN) [64] achieves high expressivity, distinguishing graph structures with a focus on injective neighborhood aggregation. GPS [48] combines GNNs with transformer-style global attention to effectively process both local and global graph structures. Similarly, GraphMamba [59] processes local structures using GNNs and leverages the Mamba module to capture global node relationships.

For explainer baselines, among statistical methods, Random Sampling (RRS) [34] serves as a simple baseline by selecting nodes or edges randomly for comparison. Personalized PageRank (PPR) [24] computes node importance by incorporating a teleportation mechanism that biases the random walk towards specific nodes, effectively capturing both local and global graph structures. Minimum Dominating Set (MDS) [44, 63] identifies a minimal set of nodes that can collectively influence or dominate all other nodes in the graph, providing insights into critical nodes for coverage or control. Notably these three statistical methods only do not use AA sequence node features. For gradient-based methods, Saliency [52] highlights features based on the magnitude of input gradients. InputXGradient [51] combines input features with their gradients to capture feature significance. Deconvolution [42] focuses on reconstructing important input features, emphasizing positive influences. ShapleyValueSampling [54] estimates feature importance using a game-theoretic approach. GuidedBackpropagation [53] refines gradients to highlight only relevant activations. From GNN-specific explainability approaches, we adopted GNNExplainer [65] to uncover subgraphs and features that are critical for predictions, and PGExplainer [39], which uses a neural network to identify significant graph components.

E METRICS

- **Fidelity+**: Fidelity+ measures how well the important features identified by the model contribute to accurate predictions. It is defined as:

$$\text{Fidelity+} = \frac{1}{N} \sum_{i=1}^N (f(G_i) - f(G_i \setminus S_i)),$$

where $f(G_i)$ is the prediction score for graph G_i , and $f(G_i \setminus S_i)$ is the prediction score after removing the subgraph S_i identified as important.

- **Fidelity-**: Fidelity- evaluates the drop in prediction accuracy when the identified important features are retained while others are removed. It is defined as:

$$\text{Fidelity-} = \frac{1}{N} \sum_{i=1}^N (f(S_i) - f(G_i)),$$

where $f(S_i)$ is the prediction score for the retained subgraph S_i , and $f(G_i)$ is the original score.

As a classic method of biological functional enrichment analysis, GO analysis evaluates whether specific biological processes, molecular functions, or cellular components are statistically over-represented in a given set of genes (i.e., gene nodes from subgraphs) compared to a background gene set [21]. The results provide a list of GO terms that highlight the biological functions most significantly represented in the input gene nodes [4]. In our study, we conducted GO enrichment analysis using the R package `clusterProfiler` [66] to identify enriched GO terms.

To assess **Breadth** of the subgraphs' biological functions, we use the Number of Enriched Biological Functions (**#EBF**) as a metric. For an input subgraph S_i , #EBF is defined as:

$$\#EBF(S_i) = |GO_{\text{enriched}}(S_i)|,$$

where S_i denotes the i -th input subgraph, $GO_{\text{enriched}}(S_i)$ is the set of significantly enriched GO terms associated with the genes in S_i , and $|GO_{\text{enriched}}(S_i)|$ is the size of the set of enriched GO terms for subgraph S_i . A high #EBF value indicates broader functional diversity within the subgraph.

To assess **Depth** of the subgraphs' biological functions, we used the Enrichment Contribution Score (**ECS**) as a metric. The ECS evaluates the relative contribution of the top-weighted genes, denoted as G_{Top} , to the enrichment of biological functions. The ECS can be assessed by following steps: Let $G = \{g_1, g_2, \dots, g_n\}$ represent the ranked list of gene nodes, sorted by their importance scores (weights) $w = \{w_1, w_2, \dots, w_n\}$, where $w_1 \geq w_2 \geq \dots \geq w_n$. Define $G_{\text{Top}} = \{g_1, g_2, \dots, g_{\text{Top}}\}$ to include only genes with the top weights, selected based on a ratio $R\%$ (defaulted as 30%), as a subset of G . Then, perform GO analysis based on G_{Top} for each input subgraph S_i . The ECS is calculated as the average number of enriched items for each gene in G_{Top} across all subgraphs S_i , and is defined as:

$$\text{ECS} = \frac{1}{P} \sum_{i=1}^P \frac{|GO_{\text{top-enriched}}(S_i)|}{|G_{\text{Top}}|},$$

where P is the total number of tested subgraphs, $GO_{\text{top-enriched}}(S_i)$ is the set of enriched GO terms for subgraph S_i based on G_{Top} , and $|G_{\text{Top}}|$ is the number of genes in the subset G_{Top} .

Table 5: PathExplainer fidelity score comparison with other classifier models.

Methods	Fidelity+	Fidelity-	(Accuracy)
GIN	0.689 ± 0.012	0.390 ± 0.008	(0.717 ± 0.013)
GPS	0.763 ± 0.017	0.529 ± 0.011	(0.726 ± 0.014)
Graph-Mamba	0.708 ± 0.015	0.430 ± 0.012	(0.723 ± 0.014)
PathMamba	0.442 ± 0.012	0.037 ± 0.008	(0.754 ± 0.015)

To assess **Reliability** of the subgraphs' biological functions, we use the well-established statistical concept **P-value** as a metric. Specifically, the P-value is calculated as the average of the P-values from statistical tests performed for biological function enrichment in each subgraph above. Since during the GO analysis, we accept the item only with a P-value lower than 0.05, the average P-value reported here is naturally lower than this threshold. A lower average P-value indicates greater reliability in the enrichment results across the subgraphs.

F ABLATION STUDY

F.1 Classifier ablation

Table 5 presents the results of PathExplainer when the classifier model is changed. In our PathMamba, the fidelity+ score is reduced to less than one-tenth, indicating that the extracted subgraph alone produces nearly identical results. This suggests that ExPath is capable of extracting biologically functional pathways sufficiently. Our PathMamba exhibits a relatively low fidelity+, which may imply that it has strong representational power, allowing it to learn meaningful representations even from subgraphs that were not extracted.

G CASE STUDY

G.1 T cell receptor (TCR) signaling pathway

The T cell receptor (TCR) signaling pathway is a cornerstone of adaptive immunity, orchestrating antigen-specific T cell activation, clonal expansion, and effector differentiation [22]. This pathway is initiated upon engagement of the TCR complex with peptide-MHC ligands, triggering a cascade of intracellular signaling events mediated by the Src-family kinases LCK and FYN, leading to phosphorylation of the immunoreceptor tyrosine-based activation motifs (ITAMs) within the CD3 and ζ -chain subunits [16]. Subsequent recruitment and activation of ZAP-70 further amplify downstream signaling through the LAT signalosome, engaging multiple adaptor proteins and second messengers that regulate key pathways, including calcium mobilization, Ras-MAPK, and NF- κ B signaling, which collectively drives gene transcription, metabolic reprogramming, and cytoskeletal remodeling necessary for T cell function [50].

Precise modulation of these signaling cascades is critical for maintaining immune homeostasis, as dysregulation is implicated in a spectrum of immune disorders, including autoimmunity, primary immunodeficiencies, and T cell malignancies, where aberrant activation or attenuation of TCR signaling disrupts immune tolerance, facilitates chronic inflammation, or drives oncogenic transformation. Analysis of the molecular intricacies of TCR signaling helps

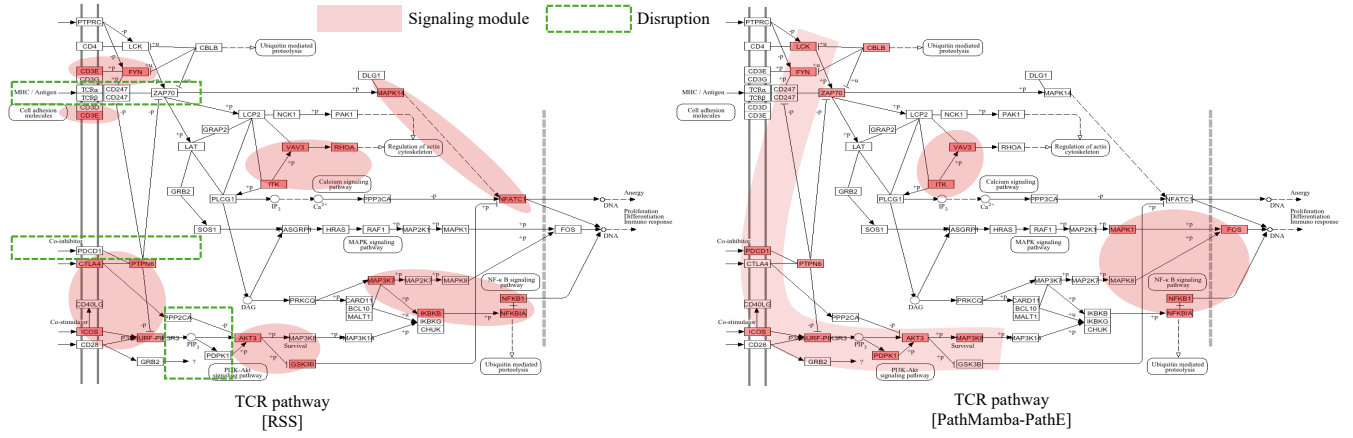


Figure 6: Comparison of subgraphs extracted from the TCR signaling pathway using two different methods. The TCR Subgraph on the left is from the RSS method, and the TCR Subgraph on the right is from the proposed method. The subgraph nodes and their signaling modules are colored in red. The disruptions within signaling paths are marked in green boxes.

therapeutic interventions, including immune checkpoint modulation, CAR-T [47] cell engineering, and small-molecule inhibitors aimed at restoring immune balance and targeting immune-related diseases.

G.2 Results and discuss

TCR Subgraph A: The RSS Method. As shown in Figure 6, the subgraph on the left, generated by the RSS method, distributes high scores uniformly across a broad range of nodes within the TCR pathway. However, this hints at unnatural, fragmented signal propagation, as highlighted by numerous discrete red-marked nodes. The absence of coherent signaling continuity, as indicated by the disrupted green-boxed regions, suggests that the method fails to prioritize biologically meaningful regulatory modules. Since its broader coverage spans multiple branches of the pathway without emphasizing critical molecular hubs, limiting its utility in pinpointing key functional perturbations.

TCR Subgraph B: The Proposed Method. In contrast, as shown in Figure 6, the subgraph on the right extracted by our method exhibits a strong focus on the PI3K-AKT signaling axis [57] and the downstream components of the NF-κB [12] pathway, as highlighted by the coherent red-marked path. These regions are believed to be crucial for regulating T cell survival, proliferation, and cytokine production [10]. Notably, the subgraph includes key regulatory genes such as *MAPK1*, *MAP3K8*, and *NFKB1* [9, 13] within a compact set of prioritized nodes. The enrichment of these molecular hubs suggests that our method effectively captures biologically significant signaling elements, aligning with well-established immune regulatory mechanisms.

In our case study, the proposed method provides a focused selection of key regulatory pathways, emphasizing PI3K-AKT and NF-κB signaling and their downstream effectors, which are crucial for modulating immune responses. In contrast, the RSS method, while providing broader pathway coverage, lacks specificity, making it less suitable for pathway analyses requiring mechanistic interpretation.